Energy & Environmental Science

Cite this: *Energy Environ. Sci.*, 2012, **5**, 7575

www.rsc.org/ees

PAPER

Self-cleaning, broadband and quasi-omnidirectional antireflective structures based on mesocrystalline rutile TiO_2 nanorod arrays†

Jinguang Cai,[a] Jianfeng Ye,[a] Suyue Chen,[a] Xiaowei Zhao,[a] Dayong Zhang,[a] Shuai Chen,[a] Yurong Ma,[a] Song Jin*[b] and Limin Qi*[a]

Received 28th December 2011, Accepted 22nd March 2012
DOI: 10.1039/c2ee03573a

We report excellent broadband and quasi-omnidirectional antireflective (AR) structures based on highly stable, self-cleaning, mesocrystalline rutile TiO_2 nanorod arrays, which were grown by a facile hydrothermal synthesis directly on Ti foils. Typically, each hierarchical nanorod is a single-crystal-like rutile TiO_2 mesocrystal comprising many [001]-oriented nanotips about 10–30 nm in diameter grown on the top of a [001]-oriented stem nanorod about 100–400 nm in diameter. These novel hierarchical mesostructures exhibit efficient suppression of reflection towards wavelengths ranging from visible to near infrared (NIR) region, with reflection <0.5% in the visible region and <2% in the NIR region, at a wide range of incident angles ranging from nearly normal to 45°. These excellent antireflection properties could be attributed to an optimized graded refractive index profile resulting from the hierarchical tips-on-rod structure of the mesocrystalline nanorods. The chemical and thermal stability of rutile TiO_2 endows the prepared mesocrystalline TiO_2 AR structures with high stability. Moreover, the AR structures exhibit useful self-cleaning properties either under UV irradiation or through fluorosilane-modification.

Introduction

Fabrication of broadband antireflective (AR) structures that can suppress reflection of light at interfaces over a broad spectral range is of great interest because reducing the reflective losses of light is crucial for improving the performance of optical and optoelectronic devices.[1–6] In this regard, AR structures including AR coatings and AR surfaces can find widespread applications ranging from solar cells[7,8] and light-emitting diodes[9] to light sensors[10,11] and miniaturized chemical analysis systems.[12] Inspired by moth-eye corneas comprising an array of nipple structures,[13] a variety of subwavelength nanostructure arrays, such as nanorod, nanowire, nanotip, nanocone, and nanopyramid arrays of polymers,[12,14–17] Si,[3,10–12,18–22] SiO_2,[23,24] III–V compounds,[25–27] and ZnO,[7,9,28,29] have been successfully fabricated as broadband AR structures. Owing to the continuous gradient transition of the refractive index from air to the substrate, such AR structures can reduce reflection at a broad range of wavelengths and angles of incidence. The polymer AR structures with a graded refractive index can be fabricated *via* nanoimprint lithography[12,14–16] and photo-lithography;[17]

[a]*Beijing National Laboratory for Molecular Sciences, State Key Laboratory for Structural Chemistry of Unstable and Stable Species, College of Chemistry, Peking University, Beijing 100871, China. E-mail: liminqi@pku.edu.cn*
[b]*Department of Chemistry, University of Wisconsin–Madison, 1101 University Avenue, Madison, Wisconsin 53706, USA. E-mail: jin@chem.wisc.edu*

† Electronic supplementary information (ESI) available. See DOI: 10.1039/c2ee03573a

Broader context

Broadband antireflective (AR) structures reducing the reflective losses of light over a broad spectral range are very useful for improving the performance of optical and optoelectronic devices including photovoltaic systems and light-emitting diodes. Inspired by the moth-eye corneas, a variety of subwavelength nanostructure arrays have been fabricated as broadband AR structures to enhance light harvesting. In this work, highly stable mesocrystalline rutile TiO_2 nanorod arrays, which adopted a unique tips-on-rod structure, were fabricated *via* a facile solution growth method. These hierarchical TiO_2 nanorod arrays provide an optimized graded refractive index profile, resulting in excellent reflection properties towards wavelengths ranging from visible to the near infrared (NIR) region at a wide range of incident angles. This study may open up a new route towards excellent AR coatings based on hierarchical nanorod arrays with optimized architectures for light harvesting.

however, their application is limited by polymer's poor stability under irradiation and at elevated temperatures. Among various inorganic materials, Si is arguably the most common material used for fabricating AR structures[5] and a large number of silicon AR surfaces with excellent broadband antireflection properties have been prepared *via* different dry etching[3,18–21] and wet etching[22] approaches. While Si AR surfaces have shown promising applications in silicon-based solar cells, their application is largely limited to the silicon-based devices; moreover, silicon is not transparent for visible light and tends to be oxidized in air. There are also some reports on the top-down fabrication of SiO_2 AR coatings[23] and III–IV semiconductor AR structures,[25–27] as well as the vapor deposition of ZnO nanoarrays as AR coatings.[7,9] Generally, the top-down fabrication and vapor deposition methods require costly equipments and are time- and energy-consuming. Recently, ZnO nanostructure arrays grown from solution at a low cost have been shown as effective AR coatings;[28,29] however, ZnO is unstable in either acidic or basic solutions, severely limiting their applications. Therefore, it remains a great challenge to achieve the facile, low-cost, and high-throughput fabrication of broadband and omnidirectional AR structures based on nanoarrays of inorganic materials with high stability.

Titanium dioxide (TiO_2) is the most widely used white pigment because of its brightness, high refractive index, low cost, and excellent stability. Due to these favorable attributes, TiO_2 semiconductor is intensively investigated for applications in photocatalysis, solar cells, sensors, and biomedical devices.[30,31] Its wide energy bandgap and excellent chemical and thermal stability should also make TiO_2 a promising candidate material for AR structures. TiO_2 AR coatings have been prepared by laser sputtering,[32] magnetron sputtering,[33,34] and sol–gel methods.[35] However, such conventional single-layer AR coatings are usually limited to single wavelength and at normal incidence of light only, and gradient-refractive-index AR structures incorporating arrays of tapered elements are highly desirable owing to their broadband and quasi-omnidirectional AR properties.[5] To date, effective AR structures based solely on TiO_2 nanorod arrays have not been reported, although a graded index film consisting of TiO_2 and SiO_2 nanoarray layers was fabricated on AlN as a near-perfect AR coating by oblique-angle vapor deposition.[2] Effective AR structures solely made of TiO_2 nanoarrays may be realized if hierarchical TiO_2 nanorod arrays consisting of tapered nanotips could be prepared in an inexpensive process to achieve an optimized graded refractive index profile. Herein, we report a facile hydrothermal solution growth of novel mesocrystalline rutile TiO_2 nanorod arrays on Ti foil substrates, which exhibited efficient suppression of reflection towards wavelengths ranging from visible to the near infrared (NIR) region at a wide range of incident angles. Specifically, 2D arrays of rutile TiO_2 nanorods with a unique tips-on-rod structure were successfully synthesized, which led to an optimized graded refractive index and hence prominent broadband and quasi-omnidirectional AR properties. Moreover, the AR structures showed excellent chemical and thermal stability as well as self-cleaning properties either under UV irradiation or through fluorosilane-modification. To our knowledge, this is the first time that a broadband AR structure based solely on TiO_2 nanoarrays has been realized.

Experimental

Materials and synthesis

Concentrated hydrochloric acid (HCl) (36–38% by weight) and tetrabutyl titanate (TBT) were purchased from Beijing Chemical Reagent Co. and Beijing Yili Chemical Reagent Co., respectively, and used without further purification. Titanium foils (99.7%, Sigma-Aldrich) approximately 250 μm thick were initially cleaned by sonication in acetone, ethanol, subsequently rinsed with deionized (DI) water, and finally dried in air. TiO_2 nanorod arrays were grown on Ti foils in an aqueous HCl solution of TBT under hydrothermal conditions. In a typical synthesis, a square titanium foil (~1.2 cm × 1.2 cm) was placed in a Teflon-lined stainless steel autoclave (20 mL), containing a solution of 6 mL of deionized water, 6 mL of concentrated HCl, and 0.5 mL of TBT, which was then heated at 150 °C for 20 h. After the autoclave cooled to room temperature, the substrate was taken out and cleaned with DI water, and then dried in a 60 °C oven in air.

Structural characterization

The products were characterized by powder X-ray diffraction (XRD, Rigaku Dmax-2000, Cu Kα radiation), scanning electron microscopy (SEM, Hitachi S4800, 5 kV), transmission electron microscopy (TEM) and high-resolution TEM (HRTEM, FEI Tecnai F30, 300 kV).

Optical reflection measurement

The measurement of specular reflection spectra in the wavelength range 400–2400 nm was performed using a Lambda 950 spectrometer (PerkinElmer) containing a halogen and a deuterium lamp, in combination with a photomultiplier for visible light and a PbS detector for infrared light. A special rotation sample stage was adopted to change the angle of incidence for the measurement of angle-resolved specular reflection spectra.

Self-cleaning experiments

The self-cleaning properties of the TiO_2 nanorod array structures were demonstrated using two approaches. First, after calcination at 400 °C for 2 h, the substrate was immersed in a 1 mM solution of 1*H*,1*H*,2*H*,2*H*-perfluorodecyltrichlorosilane (Alfa Aesar) in hexane overnight at room temperature. The resulting surface was rinsed with dichloromethane and then dried in air. The contact angle (CA) of water on the surface was measured using an OCA20 contact angle measuring system (Dataphysics). Second, oleic acid was used as a mock organic contaminant to illustrate the photocatalytic cleaning under UV irradiation. The surface of the antireflection structures was contaminated by dipping into a concentration of 1 wt% oleic acid solution in acetone. Then, the substrate coated with oleic acid was placed under UV light (365 nm, 3.8 mW cm^{-2}) for 6 h and then the water contact angles were measured again to evaluate the effect of cleaning due to photocatalysis.

Results and discussion

A facile and large scale solution growth of TiO_2 nanostructures first needs to be developed for enabling the broadband AR

structures. We were inspired by several recent developments in solution synthesis of TiO_2 nanowires, where simple solvothermal syntheses of rutile TiO_2 nanowire arrays have been achieved from a toluene–water mixture[36] or aqueous solutions[37] directly onto transparent fluorine-doped tin oxide (FTO) substrates. Furthermore, we desire more complex hierarchical nanostructures to further enhance the light absorption or anti-reflective performance.[38] This could be achieved by forming mesocrystalline TiO_2 as part of the AR structures. Mesocrystals are assemblies of crystallographically oriented nanocrystals.[39,40] Although nanoporous anatase TiO_2 mesocrystals[41] and rutile TiO_2 mesocrystals consisting of radially aligned nanorods[42,43] or parallel nanowires[44] have been reported, the preparation of two-dimensional (2D) arrays of mesocrystalline TiO_2 nanorods has not been realized yet. In this work, the hydrothermal growth of the mesocrystalline rutile TiO_2 nanorod arrays directly on a titanium foil was readily achieved in an aqueous solution of tetrabutyl titanate (TBT) and HCl at 150 °C.

Morphology and structure

Fig. 1 shows SEM, TEM, and HRTEM images of rutile TiO_2 nanorod arrays grown on Ti foil at 150 °C for 20 h together with an optical photograph of the square Ti foil. The optical photograph shows that the whole Ti foil became dark black (Fig. 1a inset) after the growth of rutile TiO_2 nanorod arrays, preliminarily indicating efficient suppression of reflection. As shown in Fig. 2, the XRD patterns of the as-prepared nanoarray film grown on Ti foil at various stages of the growth suggest the continuous growth of pure rutile TiO_2 crystals (JCPDS no. 21-1276) on the Ti substrate. The significantly enhanced (002) diffraction peak as growth time increases indicates that the nanorod arrays are highly oriented toward the substrate surface with the [001]-oriented nanorods approximately perpendicular to the substrate surface. It can be seen from Fig. 1a that the nanorod arrays are very uniform on a large area and have no obvious defects. Further magnified SEM images (Fig. 1b and c) reveal that the densely aligned nanorods exhibit rough top surfaces and they are not very uniform in diameter, typically ranging from 100 nm to 400 nm and further that the nanorods are separated by gaps and there are numerous nanotips about 10–30 nm in diameter grown vertically on the top of the stem nanorod. The cross-sectional SEM image (Fig. 1d) shows that the nanorod arrays are ~4 μm in thickness, and the nanorods are separated in the middle and upper parts of the nanoarrays, whereas some fusion appears at the bottom. This is further confirmed by the TEM image (Fig. 1e): each nanorod consists of parallel tiny nanotips about 10–30 nm in diameter and 50–200 nm in length grown on the top surface of the stem nanorod. The selected area electron diffraction (SAED) pattern corresponding to the upper part of a single nanorod displays a single-crystalline diffraction feature of rutile TiO_2, which indicates that each nanorod is a [001]-oriented, single-crystal-like, rutile TiO_2 mesocrystal consisting of many nanotips grown on the top of the [001]-oriented stem nanorod along the growth direction of the whole nanorod, in good agreement with the XRD result. The HRTEM (Fig. 1f) confirms that each nanotip is a [001]-oriented single crystal elongated along the axial direction of the nanorod. These results demonstrate the formation of the unique 2D arrays of mesocrystalline rutile TiO_2 nanorods consisting of numerous parallel nanotips grown on the top of individual nanorods.

The growth process of the mesocrystalline rutile TiO_2 nanorod arrays was investigated by examining the earlier stages of their formation at 150 °C (Fig. 3). It was observed that the nanorods began to grow on the substrate after 1 h of reaction. The nanorods grown for 2 h had a length of ~1 μm and a diameter of ~100 nm, and they were mostly grown perpendicular to the substrate with relatively smooth top surfaces (Fig. 3a and b). After 8 h of reaction, the length of the nanorods was rapidly increased to ~4 μm, and the diameter was expanded somewhat (typically 100–400 nm), as shown in Fig. 3c and d. Notably, the

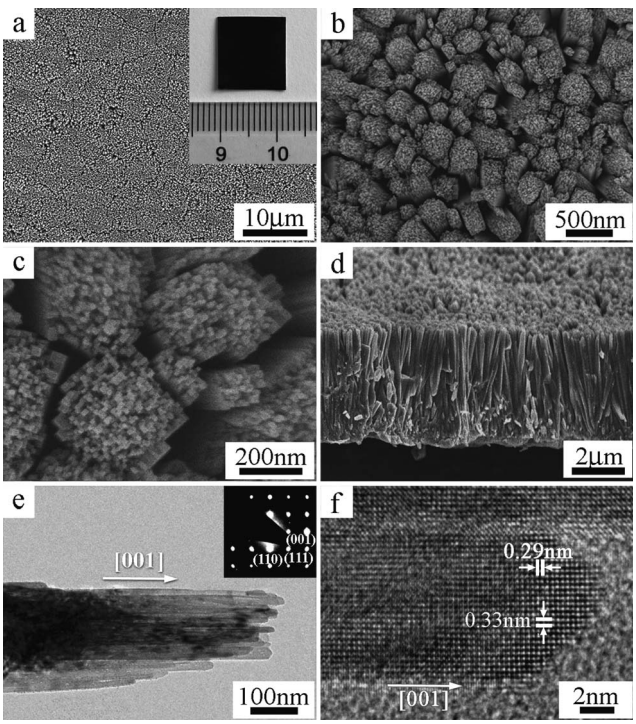

Fig. 1 (a–d) SEM, (e) TEM and (f) HRTEM images of rutile TiO_2 nanorod arrays grown at 150 °C on Ti foil for 20 h. The inset in (a) shows the optical photograph of the Ti foil after growth. The inset in (e) shows the corresponding SAED image.

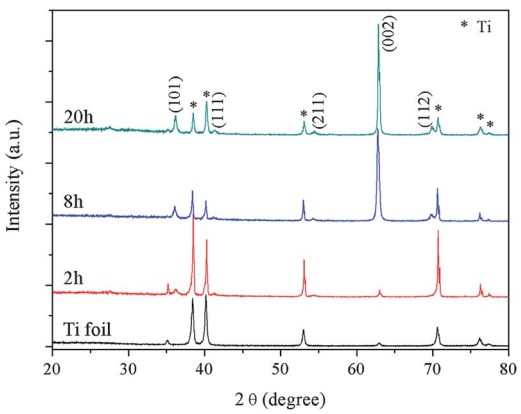

Fig. 2 XRD patterns of bare Ti foil and rutile TiO_2 nanorod arrays grown on Ti foils at 150 °C for different times.

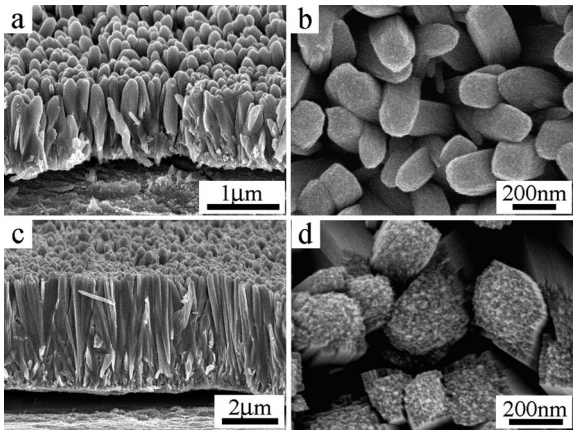

Fig. 3 Cross-sectional view (a and c) and top view (b and d) SEM images of rutile TiO_2 nanorod arrays grown on Ti foils at 150 °C for different times: (a and b) 2 h and (c and d) 8 h.

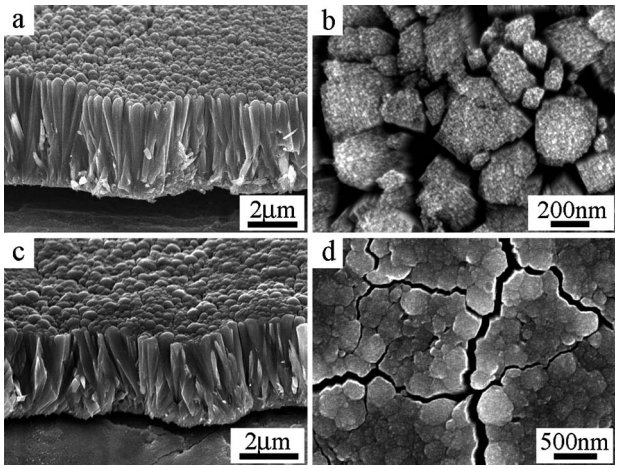

Fig. 4 Cross-sectional view (a and c) and top view (b and d) SEM images of rutile TiO_2 nanorod arrays grown on Ti foils for 20 h at different reaction temperatures: (a and b) 140 °C and (c and d) 120 °C.

top surface of the nanorods became quite rough and many step edges (about several nanometres to several tens of nanometres in height) appeared, which looked like the nanotips formed after 20 h but were much shorter. When the reaction time was further increased to 20 h, the step edges were elongated to form the parallel nanotips with lengths in the range of about 50–200 nm while the length of the stem nanorods remained essentially unchanged. It may be noted that similar step edges were previously observed on the top of the rutile TiO_2 nanorod arrays grown on FTO but the evolution of the step edges into the elongated nanotips was not observed.[37] Moreover, the current nanoarray films are tightly adhered to the Ti substrate, whereas the rutile TiO_2 nanoarray films hydrothermally grown on other substrates were easily peeled off from the substrates.[37] The adhesion of TiO_2 film on the substrate is a key issue for their applications in dye-sensitized solar cells (DSSCs).[45] The adherence of the TiO_2 nanorod arrays was further examined by heating the Ti foil with the nanoarrays in aqueous NaCl solution and subsequent peel-off test employing Scotch tape, which confirmed the adherence reliability of the TiO_2 layer on the Ti substrate (Fig. S1, ESI†).

The growth of the nanorod arrays on Ti foils is very sensitive to the reaction temperature. When the temperature was increased to above 160 °C, the Ti foils react with HCl and dissolve in the solution rapidly due to superhigh acidity. TiO_2 nanorod array films can grow on the Ti substrates at lower temperatures, but the interspace between nanorods and the thickness of the film would decrease with lowering temperature. When the temperature was decreased to 140 °C, the film thickness was reduced slightly to about 3.5 μm and the interspace between nanorods decreased slightly as well (Fig. 4a and b). The top surface of the nanorods is rough and contains many step edges. At 120 °C, the thickness was reduced to about 2.5 μm, and the nanorod arrays were too dense for identifying each nanorod individually (Fig. 4c and d). The TiO_2 thin film obtained at 120 °C exhibited obvious cracks (Fig. 4d), which is in contrast to the almost crack-free TiO_2 nanorod arrays obtained at 150 °C, suggesting that the stresses during the drying process were difficult to release for the dense thin film obtained at the lower temperature. When the temperature was further decreased to 100 °C, a very dense thin film was grown on the Ti substrate (Fig. S2, ESI†). The corresponding XRD patterns indicate that the films grown above 100 °C are still all rutile TiO_2 crystals, and the relatively enhanced intensity of (001) diffraction peak suggests the similar anisotropic growth along the [001] direction (Fig. S3, ESI†).

Growth mechanism

Based on the time-dependent investigation, we proposed a tentative growth mechanism of the mesocrystalline rutile TiO_2 nanorod arrays as follows. When tetrabutyl titanate (TBT) was mixed with HCl solution at room temperature, TBT reacted with HCl and H_2O forming Ti(IV) complex. When the solution was heated, the Ti(IV) complex transformed to TiO_2 on the surface of Ti foil. The Cl^- ion can selectively adsorb onto the {110} crystal planes suppressing further growth of the planes, resulting in the anisotropic growth along the [001] direction.[46] Meanwhile, the growth process was significantly influenced by the concentration of the Ti(IV) complex in the solution. Initially, the nanorods grew rapidly along [001] direction due to the high reactant concentration. As the reaction proceeded, the reactant concentration was reduced to a low level, and small nanotips began to grow on the stem nanorods with continuous crystal lattices, resulting in the final mesocrystalline rutile TiO_2 nanorods with a hierarchical structure. It is also possible that the precursor concentrations are depleted at the end of the hydrothermal reactions so the reaction supersaturation is low, which can be conducive for forming thinner nanorods during the hydrolysis reaction forming TiO_2.[47,48] As described above, the reaction temperature also played an important role in the formation of the rutile TiO_2 nanorod arrays on the Ti foil substrate. When the temperature was higher than 160 °C, Ti foil reacted with HCl to form Ti^{3+} ions, leading to the dissolution of the Ti foil. On the other hand, with decreasing reaction temperature, the thickness of the as-prepared films and the interspace between nanorods are reduced gradually, and the tiny tips on the top surface of the nanorods tend to disappear, leading to the formation of dense films rather than nanorod arrays at temperatures below 120 °C. This result may be rationalized by considering that the reaction for the TiO_2

formation was so slow at the low temperatures that the reaction rate was lower than the diffusion rate of the reacting titanium species, thus favoring the slow growth of dense TiO_2 films rather than anisotropic growth of separated TiO_2 nanorods. Therefore, an appropriate reaction temperature (*e.g.*, 150 °C) and a long enough growth time (*e.g.*, larger than 15 h) were crucial for the formation of the mesocrystalline rutile TiO_2 nanorod arrays on Ti foil.

Antireflection properties

The AR properties of the rutile TiO_2 nanorod arrays grown on Ti foil at 150 °C for different times were investigated by measuring their specular reflection spectra in the broad wavelength range of 400–2400 nm. Fig. 5a shows the specular reflection spectra of the as-prepared nanoarray films on Ti foils with different growth times at an incident angle of 6°. The reflection spectrum of Ti foil without polishing exhibits 10–20% for the visible region and 20–40% for the NIR region ranging from 800 to 2400 nm. The reflection was gradually suppressed as rutile TiO_2 nanorod arrays were grown on the Ti foil. The nanorod arrays grown for 2 h, which were ~1 μm in length and exhibited relatively smooth top surfaces, show an obvious suppression of reflection towards both the visible and the NIR region (red circles) with reflection <3% and <10%, respectively. When the growth time was extended to 8 h, the reflection (green triangles) is further reduced to <1% for the visible region and <5% for the NIR region, owing to the formation of arrays of nanorods ~4 μm in length with obvious step edges on the top surfaces. When the growth time was further increased to 20 h, the typical mesocrystalline rutile TiO_2 nanorod arrays consisting of nanotips (~10 to 30 nm in diameter) grown on stem nanorods were formed, and the reflection (blue triangles) is significantly suppressed, with reflection <0.5% in the visible region and <1.5% in the NIR region. This can be seen more clearly from the enlarged spectrum shown in Fig. 5b.

Moreover, the specular reflection spectra of the mesocrystalline rutile TiO_2 nanorod arrays at different angles of incidence were measured to reveal their omnidirectional antireflection properties, which are shown in Fig. 5b. It is clear that the mesocrystalline nanorod arrays exhibit prominent antireflection performance toward wide angles of incidence from 6° (nearly normal to the substrate) to 45° with reflection <2% in the broad wavelength range of 400–2400 nm. The reflection remained to be less than 2% in the wavelength range 400–800 nm when the incidence angle was further increased up to 60° (Fig. S4, ESI†), indicating typical broad-angle or quasi-omnidirectional AR properties.[3,25,26] Therefore, the mesocrystalline rutile TiO_2 nanorod array film represents an excellent broadband and quasi-omnidirectional AR structure, which could be attributed to an optimized graded refractive index profile resulting from the hierarchical tips-on-rod structure of the mesocrystalline nanorods. Surprisingly, the AR properties of the solution grown mesocrystalline rutile TiO_2 nanorod arrays are comparable to those of many Si AR surfaces with a nanoarray structure that have been fabricated by sophisticated methods.[19–22] This result demonstrates that the use of the mundane TiO_2 material can be tuned from typical white pigments to dark black AR coatings through rational tailoring of its morphology and nanoarchitecture. It may be reasonably expected that the obtained Ti foil-supported TiO_2 nanorod arrays with prominent AR properties could be directly used as a useful substrate for the visible and NIR laser desorption ionization mass spectrometry (LDI-MS) with lower laser powers.[12,49,50]

The key role of the hierarchical tips-on-rod structure in the AR property was further demonstrated by measuring the antireflection performance of the TiO_2 nanorod arrays obtained at lower reaction temperatures. As shown in Fig. 6, the reflection of the nanorod array films obtained at 140 °C was increased to about 1% and 8% from 0.4% and 1.5% for the typical hierarchical

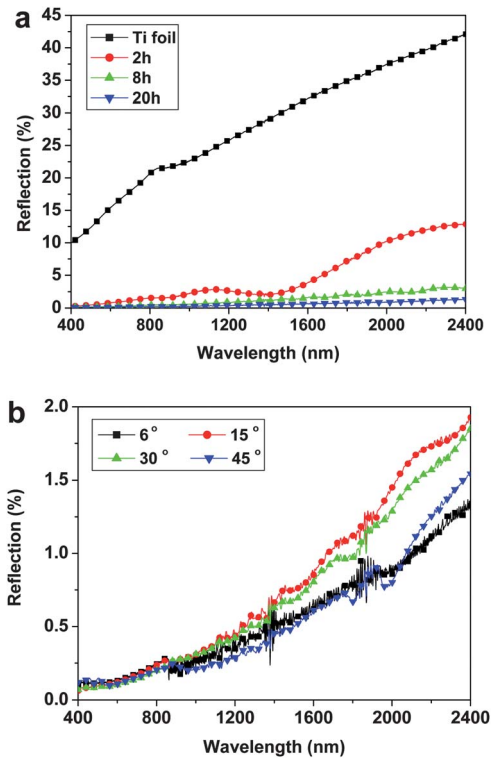

Fig. 5 (a) Specular reflectance spectra of rutile TiO_2 nanorod arrays grown on Ti foils for different times at an incident angle of 6°. (b) Specular reflectance spectra of rutile TiO_2 nanorod arrays grown on Ti foils for 20 h at different angles of incidence.

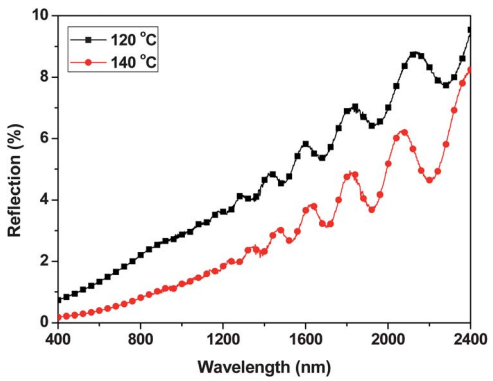

Fig. 6 Specular reflectance spectra of rutile TiO_2 nanorod arrays grown on Ti foils at different temperatures for 20 h at an incident angle of 6°.

nanorod array films obtained at 150 °C at the wavelength of 800 nm and 2400 nm, respectively. Moreover, obvious interference fringes appeared in the reflectance spectrum owing to the disappearance of highly tapered nanotips.[6] The reflection was further increased to about 2% and 10% at the wavelength of 800 nm and 2400 nm for the films grown at 120 °C. These phenomena can be easily understood from the view of the refractive index change of the films. The nanorod arrays obtained at the low temperatures are too dense to give desirable graded refractive index profiles, resulting in relatively poor AR properties.

Flexibility and stability

It is noteworthy that the growth of the mesocrystalline rutile TiO_2 nanorod arrays is independent of the shapes of the Ti foils. For example, TiO_2 nanorod arrays can be grown on Ti foils with different shapes and curvatures, producing dark black AR foils with arbitrary shapes (Fig. S5, ESI†). Moreover, when the Ti foil with rutile TiO_2 nanorod arrays was slightly bent, no apparent changes were observed for individual nanorod arrays and just blocks of nanorod arrays were separated from each other to release the stress (Fig. S6, ESI†). Therefore, this facile growth method combined with the flexibility and the processing techniques of the Ti metal could enable the AR structures consisting of rutile TiO_2 nanorod arrays grown on the Ti substrate to be used widely. It is noteworthy that efficient flexible DSSCs have been fabricated by deposition of TiO_2 nanoparticles[51] or growth of TiO_2 nanorods[52] on a Ti-foil substrate for the photo-anode and using a transparent counter-electrode. Therefore, the current mesocrystalline rutile TiO_2 nanorod arrays on Ti substrate with excellent AR properties could become a promising candidate as the photo-anode in flexible DSSCs with enhanced performance of light harvesting.

As expected, the chemical and thermal stability of rutile TiO_2 endows the prepared AR structures based on the mesocrystalline rutile TiO_2 nanorod arrays with excellent stability. For example, after the as-prepared nanorod array film was immersed in a 2 M NaOH solution at room temperature for 2 h, there were no considerable changes for both the nanoarray structure and the AR properties (Fig. S7, ESI†). Similarly, immersing in 6 M HCl for 2 h did not cause any considerable changes for the AR structures. Moreover, after calcination at 500 °C for 1 h, the nanorod arrays maintained the same morphologies and exhibited excellent antireflection performance despite a slight increase of reflection compared with the as-prepared sample (Fig. S8, ESI†). Therefore, the AR structures based on the mesocrystalline rutile TiO_2 nanorod arrays have excellent chemical and thermal stability, which makes them promising candidates for long-term applications in complicated or extreme environments.

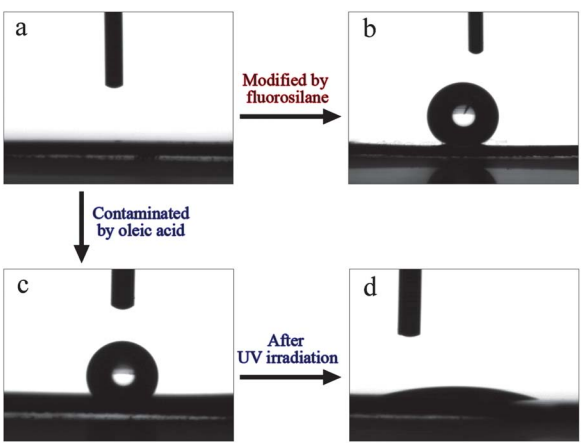

Fig. 7 Scheme for self-cleaning processes. (a) Water drop profile on calcined TiO_2 nanorod arrays. (b) Water drop profile on fluorosilane-modified TiO_2 nanorod arrays. (c) Water drop profile on TiO_2 nanorod arrays contaminated by oleic acid. (d) Water drop profile on TiO_2 nanorod arrays after UV irradiation following the contamination.

Self-cleaning properties

Self-cleaning properties of AR structures are also important in practice because they can potentially save the time and cost of cleaning and maintenance. The self-cleaning properties of the TiO_2 nanoarray-based AR structure were investigated by two different ways, namely, superhydrophobicity[19] and photocatalysis.[53] The as-prepared nanorod arrays were first calcined at 400 °C for 2 h, exhibiting a superhydrophilic surface with a water contact angle nearly 0° (Fig. 7a). For the superhydrophobicity-based self-cleaning, 1*H*,1*H*,2*H*,2*H*-perfluorodecyltrichlorosilane was used to modify the surface of the nanorod arrays, resulting in a significant increase of the water contact angle to ~161° (Fig. 7b). The modified surface became superhydrophobic, representing a good self-cleaning capability. Moreover, the fluorosilane modification did not cause considerable changes in the reflection of the TiO_2 nanorod arrays, suggesting a good preservation of the AR properties (Fig. S9, ESI†). For the photocatalysis-based self-cleaning, the photocatalytic degradation of oleic acid, which was used as a mock organic contaminant, was carried out and the contact angle of the AR film was measured to evaluate the self-cleaning properties.[53] After contamination of the calcined AR film by oleic acid, the film lost its superhydrophilicity and the water contact angle was increased to ~123° (Fig. 7c). After irradiating by UV light for 6 h, the water contact angle was decreased to ~12° (Fig. 7d), indicating that the AR structure exhibits excellent self-cleaning properties under UV irradiation. Therefore, the TiO_2 nanorod array-based AR films can display self-cleaning capability either by modifying with fluorosilane or under UV irradiation, which may find applications under different practical situations. It may be noted that similar self-cleaning properties have been reported for the self-organized TiO_2 nanotube layers grown on Ti substrate by electrochemical anodization.[54] In the current situation, the self-cleaning properties can provide additional benefits for the mesocrystalline TiO_2 nanorod arrays when they are used as efficient AR surfaces in natural or complicated environments.

Conclusions

In conclusion, novel mesocrystalline rutile TiO_2 nanorod arrays consisting of parallel nanotips grown on the top of individual nanorods were successfully grown on Ti foils by a facile hydrothermal synthesis. It was demonstrated that the obtained TiO_2 nanorod arrays on Ti foils exhibited excellent broadband and quasi-omnidirectional antireflection performance, which may be

ascribed to the optimized graded refractive index profile owing to the mesocrystalline nanorod arrays with a hierarchical tips-on-rod structure. The rutile TiO_2 nanorod array-based AR films showed excellent chemical and thermal stability and useful self-cleaning properties either under UV irradiation or through fluorosilane-modification. The highly stable, self-cleaning, broadband AR structures based on rutile TiO_2 nanorod arrays may find potential applications including solar cells, displays, and chemical sensors with improved efficiency. This study may open up a new route towards excellent AR coatings based on hierarchical nanorod arrays with optimized architectures for light harvesting.

Acknowledgements

This work was supported by NSFC (21073005, 21173010, and 50821061) and MOST (2007CB936201). The authors thank Dr Mingzhu Li for beneficial discussion on reflectance spectra. S.J. thanks U.S. NSF Grant (DMR-1106184), the Sloan Research Fellowship and the Research Corporation SciaLog Award for support.

Notes and references

1 J. A. Hiller, J. D. Mendelsohn and M. F. Rubner, *Nat. Mater.*, 2002, **1**, 59–63.
2 J. Q. Xi, M. F. Schubert, J. K. Kim, E. F. Schubert, M. Chen, S.-Y. Lin, W. Liu and J. A. Smart, *Nat. Photonics*, 2007, **1**, 176–179.
3 Y. F. Huang, S. Chattopadhyay, Y. J. Jen, C. Y. Peng, T. A. Liu, Y. K. Hsu, C. L. Pan, H. C. Lo, C. H. Hsu, Y. H. Chang, C. S. Lee, K. H. Chen and L. C. Chen, *Nat. Nanotechnol.*, 2007, **2**, 770–774.
4 Y. F. Li, J. H. Zhang and B. Yang, *Nano Today*, 2010, **5**, 117–127.
5 S. Chattopadhyay, Y. F. Huang, Y. J. Jen, A. Ganguly, K. H. Chen and L. C. Chen, *Mater. Sci. Eng., R*, 2010, **69**, 1–35.
6 H. K. Raut, V. A. Ganesh, A. S. Nairb and S. Ramakrishna, *Energy Environ. Sci.*, 2011, **4**, 3779–3804.
7 Y. J. Lee, D. S. Ruby, D. W. Peters, B. B. McKenzie and J. W. P. Hsu, *Nano Lett.*, 2008, **8**, 1501–1505.
8 J. Zhu, C.-M. Hsu, Z. Yu, S. Fan and Y. Cui, *Nano Lett.*, 2010, **10**, 1979–1984.
9 S. J. An, J. H. Chae, G.-C. Yi and G. H. Park, *Appl. Phys. Lett.*, 2008, **92**, 121108.
10 C. Lee, S. Y. Bae, S. Mobasser and H. Manohara, *Nano Lett.*, 2005, **5**, 2438–2442.
11 T. Glaser, A. Ihring, W. Morgenroth, N. Seifert, S. Schröter and V. Baier, *Microsyst. Technol.*, 2005, **11**, 86–90.
12 L. Sainiemi, V. Jokinen, A. Shah, M. Shpak, S. Aura, P. Suvanto and S. Franssila, *Adv. Mater.*, 2011, **23**, 122–126.
13 P. Vukusic and J. R. Sambles, *Nature*, 2003, **424**, 852–855.
14 H. J. Gao, Z. Liu, J. Zhang, G. M. Zhang and G. Y. Xie, *Appl. Phys. Lett.*, 2007, **90**, 123115.
15 Q. Chen, G. Hubbard, P. A. Shields, C. Liu, D. W. E. Allsopp, W. N. Wang and S. Abbott, *Appl. Phys. Lett.*, 2009, **94**, 263118.
16 D.-H. Ko, J. R. Tumbleston, K. J. Henderson, L. E. Euliss, J. M. DeSimone, R. Lopez and E. T. Samulski, *Soft Matter*, 2011, **7**, 6404–6407.
17 J. Park, S. Yoon, K. Kang and S. Jeon, *Small*, 2010, **6**, 1981–1985.
18 J. Zhu, Z. Yu, G. F. Burkhard, C.-M. Hsu, S. T. Connor, Y. Xu, Q. Wang, M. McGehee, S. Fan and Y. Cui, *Nano Lett.*, 2008, **9**, 279–282.
19 W.-L. Min, B. Jiang and P. Jiang, *Adv. Mater.*, 2008, **20**, 3914–3918.
20 D. A. P. Qi, N. Lu, H. B. Xu, B. J. Yang, C. Y. Huang, M. J. Xu, L. G. Gao, Z. X. Wang and L. F. Chi, *Langmuir*, 2009, **25**, 7769–7772.
21 S. J. Cho, T. An, J. Y. Kim, J. Sung and G. Lim, *Chem. Commun.*, 2011, **47**, 6108–6110.
22 Y. F. Li, J. H. Zhang, S. J. Zhu, H. P. Dong, Z. H. Wang, Z. Q. Sun, J. R. Guo and B. Yang, *J. Mater. Chem.*, 2009, **19**, 1806–1810.
23 Y. Li, J. Zhang, S. Zhu, H. Dong, F. Jia, Z. Wang, Z. Sun, L. Zhang, Y. Li, H. Li, W. Xu and B. Yang, *Adv. Mater.*, 2009, **21**, 4731–4734.
24 Y. M. Song, H. J. Choi, J. S. Yu and Y. T. Lee, *Opt. Express*, 2010, **18**, 13063–13071.
25 C. H. Chiu, P. C. Yu, H. C. Kuo, C. C. Chen, T. C. Lu, S. C. Wang, S. H. Hsu, Y. J. Cheng and Y. C. Chang, *Opt. Express*, 2008, **16**, 8748–8754.
26 S. L. Diedenhofen, G. Vecchi, R. E. Algra, A. Hartsuiker, O. L. Muskens, G. Immink, E. Bakkers, W. L. Vos and J. G. Rivas, *Adv. Mater.*, 2009, **21**, 973–978.
27 Y. M. Song, S. J. Jang, J. S. Yu and Y. T. Lee, *Small*, 2010, **6**, 984–987.
28 Y. S. Tian, C. G. Hu, Y. F. Xiong, B. Y. Wan, C. H. Xia, X. S. He and H. Liu, *J. Phys. Chem. C*, 2010, **114**, 10265–10269.
29 Y.-C. Chao, C.-Y. Chen, C.-A. Lin and J.-H. He, *Energy Environ. Sci.*, 2011, **4**, 3436–3441.
30 X. Chen and S. S. Mao, *Chem. Rev.*, 2007, **107**, 2891–2959.
31 P. Roy, S. Berger and P. Schmuki, *Angew. Chem., Int. Ed.*, 2011, **50**, 2904–2939.
32 H.-A. Durand, J.-H. Brimaud, O. Hellman, H. Shibata, S. Sakuragi, Y. Makita, D. Gesbert and P. Meyrueis, *Appl. Surf. Sci.*, 1995, **86**, 122–127.
33 T. M. R. Viseu, B. Almeida, M. Stchakovsky, B. Drevillon, M. I. C. Ferreira and J. B. Sousa, *Thin Solid Films*, 2001, **401**, 216–224.
34 S. Tanemuraa, L. Miao, P. Jin, K. Kaneko, A. Terai and N. Nabatova-Gabain, *Appl. Surf. Sci.*, 2003, **212–213**, 654–660.
35 J. Shen, T. Yang, Q. Zhang, J. Wang and Q. Zhang, *J. Sol-Gel Sci. Technol.*, 2003, **26**, 1029–1032.
36 X. Feng, K. Shankar, O. K. Varghese, M. Paulose, T. J. Latempa and C. A. Grimes, *Nano Lett.*, 2008, **8**, 3781–3786.
37 B. Liu and E. S. Aydil, *J. Am. Chem. Soc.*, 2009, **131**, 3985–3990.
38 M. J. Bierman and S. Jin, *Energy Environ. Sci.*, 2009, **2**, 1050–1059.
39 H. Cölfen and M. Antonietti, *Angew. Chem., Int. Ed.*, 2005, **44**, 5576–5591.
40 R.-Q. Song and H. Cölfen, *Adv. Mater.*, 2010, **22**, 1301–1330.
41 J. Ye, W. Liu, J. Cai, S. Chen, X. Zhao, H. Zhou and L. Qi, *J. Am. Chem. Soc.*, 2010, **133**, 933–940.
42 S.-J. Liu, J.-Y. Gong, B. Hu and S.-H. Yu, *Cryst. Growth Des.*, 2008, **9**, 203–209.
43 D. Zhang, G. Li, F. Wang and J. C. Yu, *CrystEngComm*, 2010, **12**, 1759–1763.
44 Z. Hong, M. Wei, T. Lan, L. Jiang and G. Cao, *Energy Environ. Sci.*, 2012, **5**, 5408–5413.
45 A. S. Nair, Z. Peining, V. J. Babu, Y. Shengyuan and S. Ramakrishnab, *Phys. Chem. Chem. Phys.*, 2011, **13**, 21248–21261.
46 A. Kumar, A. R. Madaria and C. Zhou, *J. Phys. Chem. C*, 2010, **114**, 7787–7792.
47 S. Jin, M. J. Bierman and S. A. Morin, *J. Phys. Chem. Lett.*, 2010, **1**, 1472–1480.
48 F. Meng, S. A. Morin and S. Jin, *J. Am. Chem. Soc.*, 2011, **133**, 8408–8411.
49 C.-Y. Lo, J.-Y. Lin, W.-Y. Chen, C.-T. Chen and Y.-C. Chen, *J. Am. Soc. Mass Spectrom.*, 2008, **19**, 1014–1020.
50 D. Nanjo, K. Shibamoto and T. Korenaga, *Chem. Lett.*, 2009, 142–143.
51 S. Ito, N.-L. C. Ha, G. Rothenberger, P. Liska, P. Comte, S. M. Zakeeruddin, P. Péchy, M. K. Nazeeruddin and M. Grätzel, *Chem. Commun.*, 2006, 4004–4006.
52 J.-Y. Liao, B.-X. Lei, H.-Y. Chen, D.-B. Kuang and C.-Y. Su, *Energy Environ. Sci.*, 2012, **5**, 5750–5757.
53 Z. Wu, D. Lee, M. F. Rubner and R. E. Cohen, *Small*, 2007, **3**, 1445–1451.
54 E. Balaur, J. M. Macak, L. Taveira and P. Schmuki, *Electrochem. Commun.*, 2005, **7**, 1066–1070.